The Effect of the Geometric Parameters on the Air Flow Distribution Uniformity within the Protonic Ceramic Fuel Cell Stack

J.Q. Dai, M.F. Zhu, H.Z. Zhang, J.P. Liu, D.F. Chen[*]

School of Energy and Power, Jiangsu University of Science and Technology, Zhenjiang 212003, China
[*]E-mail: dfchen@just.edu.cn

Compared with the traditional fuel cells, the protonic ceramic fuel cell (PCFC) has attracted more and more attentions due to its advantages on intermediate temperature zone. In this paper, the 3D calculated fluid dynamics model for a typical PCFC stack has been developed to study the dependence and sensitivity of the flow distribution uniformity on different geometric parameters. The result shows that although the vapors are generated within the cathode sides, enlarging the manifold radius and decreasing the cell number will greatly increase the air flow distribution uniformity of PCFC stack. Increasing the *a* factor of PCFC stack will keep decreasing the slop of the air flow distribution line. Thus, it's not like bigger *a* is better in any case. For a small/large manifold radius, the slops of the flow distributing line will changed greatly/gently, while *a* factor is adjusted. Although increasing the feed/exhaust header width will increase the flow distributing uniformity over the cathode surface of each PCFC unit, its effect on the flow distribution among the piled PCFC units is negligible.

1. INTRODUCTION

With the increasing burning and use of traditional fossil energies around the world, traditional energy crisis is becoming serious. Clear and efficient methods of energy development and application have become the hot topics of researches. Many technologies have been developed to efficiently convert and store energies within the hydrocarbon fuels. Because fuel cells are not limited by the Carnot cycle, they can directly convert chemical energies of fuels into electric energies [1-4]. According to different types of electrolytes, fuel cells can be divided into different types. Proton conductive oxide is one of the typical solid ionic conductive ceramic materials, which has significant protonic electric conductivity. Protonic ceramic fuel cell (PCFC) based on proton conductive oxide has

many advantages, compared with the traditional oxygen conducting solid oxide fuel cell (O^{2-}-SOFC) in the medium temperature range [5-8]. Because the activation energy required for proton conduction (0.3-0.6 eV) is lower than that required for oxygen ion conduction (0.8 eV) [9]. Thus, PCFC could be operated around the lower temperatures zone. PCFC can also uses a wider variety of hydrocarbons as fuel [10-13], compared with traditional proton exchange membrane fuel cells (PEMFCs) that work around the low temperature zone [14, 15], Therefore, PCFC technology is now receiving extensive attentions and researches, due to its lower temperature and better fuel adaptability.

At present, there have been many studies on PCFC electrolyte, composite cathode and anode materials. Several compositions have been proposed and their effects on ionic conductivity and electronic conductivity have been studied [16, 17]. In order to improve the performance of PCFC technology, current studies are aimed at improving the efficiency of single-layer PCFC.

For the practical application of fuel cell technologies, they are generally used in the way of stacking. In the past decades, many different structures have been developed and large-scale 3D modeling approach plays an important role in the research of new structures [18]. The establishment of fuel cell model is very effective for the studying of flow, species, heat, electrons and ions transports within the stack, in which the gas flow channel is one of the most basic factors [18, 19].

There are a lot of studies on the modeling of airflow channels, D. Chen [20] established a large scale 3D multi-physical fields model with anodes supported tubular SOFC stack and studied the air distribution characteristics of the external air flow path. Maharudrayya [21] proposed a calculation method for predicting and comparing the flow distribution and pressure drop features among various U-type and Z-type flow channels of PEMFCs. Y. Zou [22] carried out large-scale modeling for 30-layer typical SOFC, developed Z-type and U-type two models with different inlet and outlet directions, and studied the SOFC flow distribution of the two structures. It can be seen that modeling studies on airflow channels are very extensive, in which SOFCs and PEMFCs account for a large proportion in previous studies due to their early presentation and good performance [23-25]. The researches on these two types of fuel cell flow channels are mature. However, although the PCFC technology, compromise the advantages of both SOFC and PEMFC technologies, there are still many aspects worth studying and finding, such as, electrolyte with higher protonic conductivity, more durable anode and cathode materials, proper stack structures and so on. In order to improve the performance of PCFC on stack level, the cathode material and structure should be studied to obtain good performance in medium temperature environment [26]. Furthermore, unlike O^{2-}-SOFC, PCFC generates vapor on the cathode side. Thus, it is also necessary to study whether the vapor generation on the cathode side affects the flow distribution quality within the stack.

In this paper, the 3D large scale calculated fluid dynamics model for the PCFC stack with typical structure are developed firstly. Then, it will be used to study the flow distributing characteristics within the PCFC stack. Finally, the dependence and sensitivity of the flow distribution uniformity on different geometric parameters, such as the cell number, manifold radius, *a* factor, header widths and so on will be carefully studied. The research result can provide us with very helpful guides for the further development of the PCFC stack technology in the near future.

2. STACK STRUCTURE AND CFD MODEL
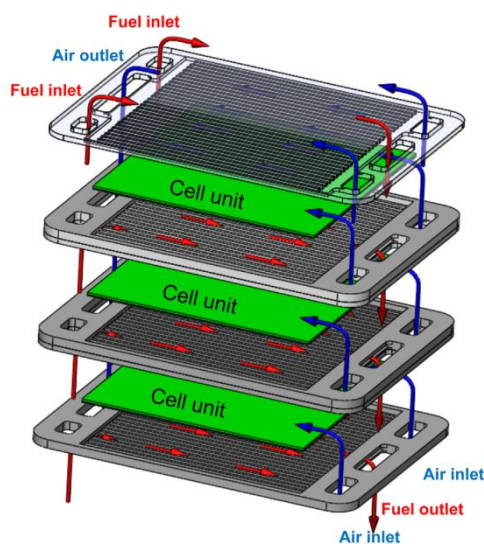
**Figure 1.** The structure of a typical planar PCFC stack [27].

Fig. 1 displays a typical stack design reported by S. Su [27] to evaluate the performance within the PCFC stack. The stack structure is constructed by fuel cell units that include anode support, anode function, dense electrolyte, cathode function and cathode current collector layers. Bipolar plates are used to connect cells in series to avoid current exposure. The cathode and anode ribs are embedded on both sides of the bipolar plate for evenly distributing the air and fuel over the cathode and anode surfaces, respectively. The inlet manifolds are also placed on bipolar plates to respectively supply the air and fuel flows to the piled cell units.

Proper air flowing and oxygen diffusing path is a key factor to ensure the high quality cathodic electrochemical reaction and heat management within the PCFC stack [20, 28]. Fig. 2 further shows the 3D model for the air flow and oxygen diffusing path of a typical 20-cells PCFC stack with the design of Fig. 1. The corresponding geometric parameters are collected in table 1, The 3D model includes: i) three inlet manifolds which fed the air flow to the piled cell units; ii) two outlet manifolds that collect the exhaust air flow and the generated vapors after the cathodic electrochemical reactions; iii) 50 rib channels to distribute the airflow over the cathode surfaces of each cell unit; iv) cathode current collector layer to prevent the serious concentration loss that might caused by the solid interconnect ribs; v) the cathode functional layer to support the cathodic electrochemical reaction $O_2 + 4H^+ + 4e^- = 2H_2O$.
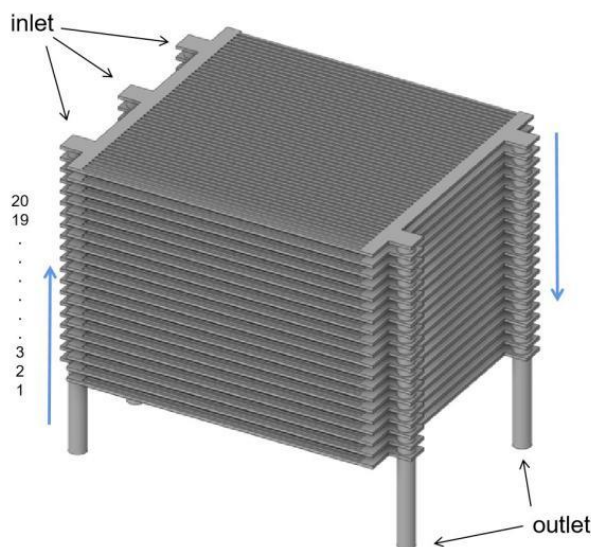
Figure 2. The 3D air flowing and oxygen diffusion path within a typical 20-cells PCFC stack.

As the entrances of the inlet manifolds and the exits of the outlet manifolds are placed on the same sides, the air flow path configuration is indicated as U-type. Fig. 3 further shows the 3D air flowing and oxygen diffusion path within a PCFC unit. It consists of the inlet manifolds, outlet manifolds, feed header, exhaust header and 50 air channels.
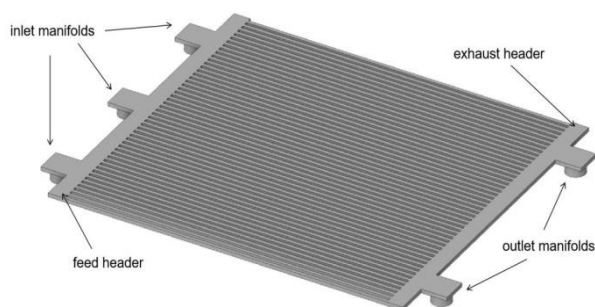
Figure 3. The 3D air flowing and oxygen diffusion path of a PCFC unit.

Table 1. The geometric and operational parameters referring to the stack structure in **Fig. 1**.

Parameters	Geometric sizes
MEA area	100×100 mm²
Single cell rib (X×Y×Z)	$1 \times 100 \times 1$ mm³
Single channel (X×Y×Z)	$1 \times 100 \times 1$ mm³
The cathode support layer thickness	0.05 mm
The cathode function layer thickness	0.01 mm
Radius of air inlet manifold	3, 4, 5, 6 mm
Radius of air outlet manifold ($r_{out}=r_{in}$)	3, 4, 5, 6 mm

Radius of air outlet manifold ($r_{out}=1.2r_{in}$)	3.6, 4.8, 6, 7.2 mm
Layer height	4 mm
Working temperature of PCFC	473 K
Output current density i_{op}	5000 A·m^{-2}
The oxygen utilization	0.2

For the 3D CFD model, continuity and momentum conservation equations are adopted to calculate the air flow within the inlet and outlet tubes and cathode rib channels.

$$\nabla \cdot (\rho \boldsymbol{u}) = 0 \tag{1}$$

$$\nabla \cdot (\rho \boldsymbol{u} \times \boldsymbol{u}) = -\nabla P + \rho \boldsymbol{f} + \mu \left(\frac{1}{3} \nabla (\nabla \cdot \boldsymbol{u}) + \Delta \boldsymbol{u} \right) \tag{2}$$

where ρ, $\boldsymbol{u}$, P are the density, velocity vector and static pressure of the fluid, respectively. μ is the effective dynamic viscosity that can be calculated by ideal air mixing law.

$$\mu = \sum_{\alpha=1}^{n} \frac{\chi_\alpha \mu_\alpha}{\sum_{\beta=1}^{n} \chi_\beta \Phi_{\alpha,\beta}} \tag{3}$$

Sutherland's Law is adopted to calculate μ_α at operation temperature *T*.

$$\frac{\mu_\alpha}{\mu_\alpha^0} \approx \left(\frac{T}{T_0} \right)^{1.5} \frac{T_0 + S}{T + S} \tag{4}$$

where μ^0 is the reference viscosity referring to T_0, S is the Sutherland constant.

The diffusion processes of oxygen, nitrogen and vapor within the rib channels, porous cathode current collector layers and cathodic functional layers can be controlled by

$$\nabla \cdot (\varepsilon \rho Y_\alpha \boldsymbol{u}) = \nabla \cdot (\rho D_{\alpha,eff} \nabla Y_\alpha) + S_\alpha \tag{5}$$

where ε is the porosity of the porous medium. Y_α and $D_{\alpha,\text{eff}}$ are the mass fraction and effective diffusion coefficient of species α, S_α is the species source item. For the cathode functional layers of PCFC stack, it can be represented as

$$S_{O_2} = -\frac{i_{op} M_{O_2}}{4Fl}, \quad S_{H_2O} = \frac{i_{op} M_{H_2O}}{2Fl}, \quad S_{N_2} = 0 \tag{6}$$

where *l* is the thickness of cathode functional layer. M_α is the molar mass of species α. *F* is the Faraday constant. The cathodic electrochemical reactions are generally agreed to be happen within the zones nearby the cathode/dense electrolyte interfaces [29]. This assumption was proved to be reasonable and its influences on the flow and species distributions within the stack were negligible [28].

The exhaust gas from rib channels of each cell unit are collected and exposed to the outlet manifold. The k-epsilon turbulence model is used for the 3D large-scale calculation. The boundary conditions of the velocity inlet and the pressure outlet are used for the stack. The rest of the boundaries are adiabatic and does not slip. The Inlet flow velocity is determined by the average current density i_{op}, stack layer number *N* and active surface area *A* to ensure proper oxygen utilization η_{O_2}.

$$u_{air}^{in} = \frac{N i_{op} A M_{air}}{4F \eta_{O_2} \chi_{O_2} \rho_{air} A_{air}} \tag{7}$$

where χ_{O_2} is the oxygen mole fraction of the feeding air flow. A_{air} is the cross-sectional area of the air inlet manifolds.

Generally, there are three essential factors to indicate the performance of the PCFC cathode air flow configurations,

a) *Minimum flow rate among the piled cells*: The stack is composed of multiple PCFC-layers in series. Thus, the performance of the stack is related to each layer and its performance is determined by the layer receiving the minimum air flow rate. The stack flow uniformity can be measured by the index U defined as $U = \min(m_1' : m_N')$. The value range of U is between 0 and 1. The better the uniformity of the stack, the higher the value of U should be.

b) *The normalized air flow rate:* The average flow $ave(m_1 : m_N)$ of each layer is also an important factor to characterize the performance of the stack and the uniformity of the air flow distribution on stack level. The normalized mass flow rate can be measured as $m_i' = \dfrac{m_i}{ave(m_1 : m_N)}$.
Generally, using normalize terms to represent flow distribution qualities makes it easy to compare the performances among stacks with different structures, sizes, or operating parameters.

c) *Stack pressure drop:* The pressure difference between the entrance of inlet manifold and the exit of the outlet manifold is also an important factor in evaluating the design quality of the stack. A large pressure drop means more additional energy loss, while a small pressure drop may result in the oxygen not being able to be supplied anywhere.

3. RESULT AND DISCUSSION

3.1 The effect of the cell numbers on the flow distributions of PCFC stack

Fig. 4 shows the distribution for 5-cells, 10-cells, 20-cells PCFC stacks, respectively. They all have 5 mm header and 3 mm radius inlet manifolds. For the 5-cells stack, *U* is 0.93, indicates that 5-cells stack is quite uniform. For the 15-cells and 20-cells stacks, *U* is decreased to 0.83 and 0.54, respectively. Obviously, for the 20-cells stack, the air flow feeding quality is far from the uniform distribution. Thus, increasing the cell number of the stack will greatly decrease the air flow distribution quality of the PCFC stacks, in which the vapors are produced within the cathode air flow path. This conclusion is quit similar with that of SOFC stack, in which a stack with smaller cell units would lead to more uniform air flow distribution [30].
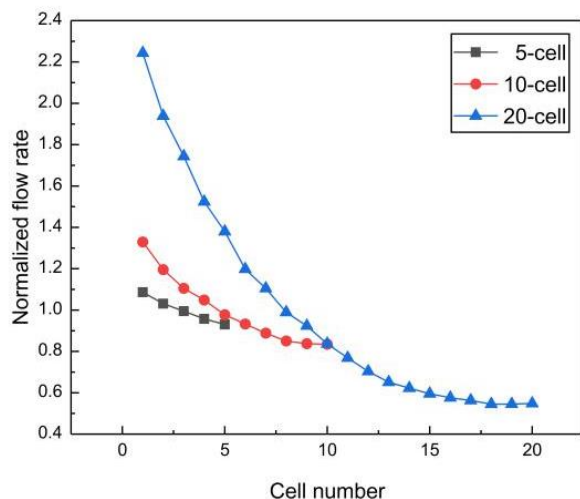
Figure 4. Comparison of the normalized flow rate distributions among the 5-cells, 10-cells and 20-cells PCFC stacks.

3.2 The influences of the manifolds radius on the PCFC performance

As discussed above, the 20-cells stack with current geometric parameters will has poor air flow distribution uniformity among the piled cell units. The sensitivity of the flow and species distributions of the PCFC stack on the geometric parameters will be investigated through the above developed 3D CFD models.
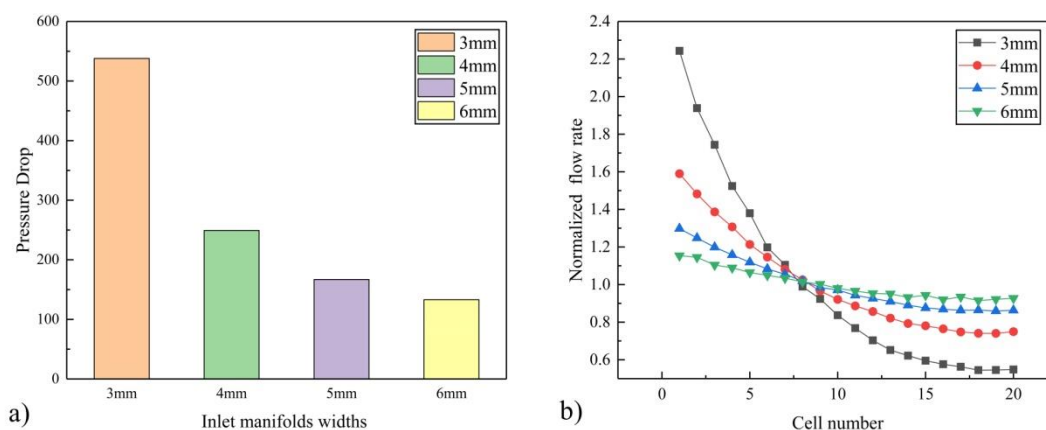

Figure 5. a) Comparison of the static pressure drops distributions of 20-cells PCFC stacks ($r_{in}=r_{out}$) with different manifold radii; b) Comparison of the corresponding normalized flow rate distributions.

Fig. 5 compare both the normalized flow rate distributions among the piled PCFC units and the corresponding stack pressure drops between the entrance of inlet manifold and the exit of the outlet manifold, while different manifold radii are adopted ($r_{in}=r_{out}$), Obviously, while the manifold radii

Int. J. Electrochem. Sci., 16 (**2021**) Article Number: 211052

8

$r_{in}=r_{out}$ is increased from 3 mm to 6 mm, the stack pressure drop will be decreased from 537 to 133 pa (shown in **Fig. 5a**).

Fig. 5b further shows the corresponding normalized air mass flow rate distribution characteristic among the piled PCFC units. Obviously, the stack uniformity U will be improved with the increasing manifolds radii. The corresponding U for the radii $r_{in}=r_{out}=$3 mm, 4 mm, 5 mm and 6 mm are 0.53, 0.74, 0.85 and 0.91, respectively. In other words, for the similar stack structure, although the PCFC stack has lower air flow distribution quality than that of SOFC stack [31], increasing the manifold radii can relief the difference of feeding air flow rates among the piled PCFC units. It can also decrease the total pressure drop throughout the whole PCFC stack.

3.3 The influences of a parameter on the PCFC performance
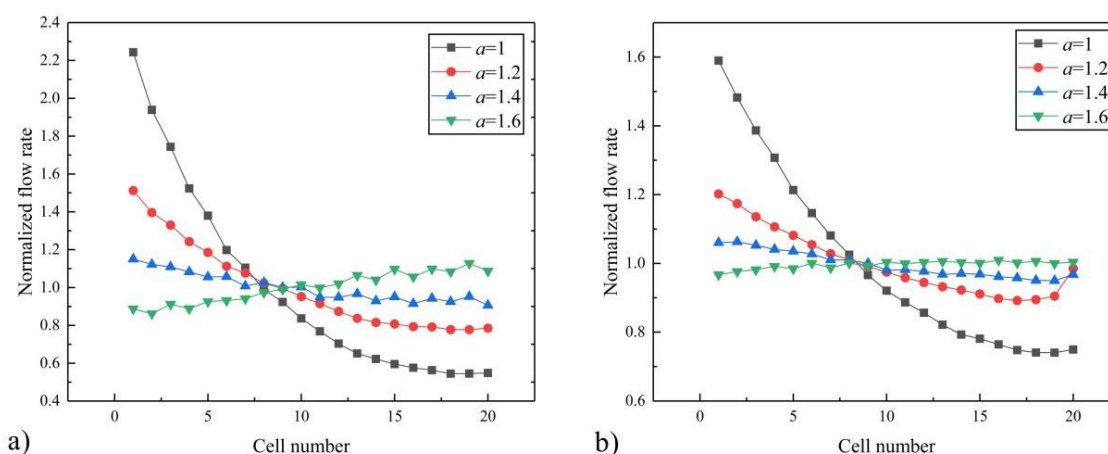
Figure 6. Comparison of the air mass flow rate distributions among those 20-cells PCFC stacks with different $a=r_{out}/r_{in}$. a) $r_{in}=$3 mm; b) $r_{in}=$4 mm.

The above section study the effect of the manifold radii on the flow distributions of PCFC stack with $a=r_{out}/r_{in}=$1. In this section, the influence of a factor on PCFC stack cathode flow distribution will be studied to find a better diameter ratio of inlet and outlet manifolds.

Selecting $r_{in}=$3 and 4 mm as the example, **Fig. 6** shows the dependence of the flow distributions of PCFC stack on factor a. From **Fig. 6a** ($r_{in}=$3 mm) we can get that U for the cases $a=$1, 1.2, 1.4, 1.6 are 0.74, 0.89, 0.95, 0.96, respectively. This result is consistent with the previous research conclusion reported by X. Bi [30], for the U-type SOFC stack, the uniformity of flow distribution will increase with the increasing a. Furthermore, the slop of the distribution lines will be decreased while a increasing; and reaches the negative value at $a=$1.6.

Similarly, **Fig. 6b** shows the effect of factor a on the flow distributing characteristics of 20-cells PCFC stack at $r_{in}=$4 mm. The corresponding U for $a=$1, 1.2, 1.4 and 1.6 are 0.74, 0.89, 0.95 and 0.96, respectively. Comparing with **Fig. 6a** and **6b**, we can get that: i) for a smaller manifold radius, the slops of the flow distributing line will changed greatly, while a factor is adjusted; ii) for a larger

manifold radius, however, the slops of the flow distributing line will changed more gently, while *a* factor is adjusted.

In **table 2,** the stack uniformity indexes *U* of 20-cells PCFC stack for different manifolds radii and *a* factors are collected. For the 20-cells PCFC stacks, the larger radius of inlet manifold the higher uniformity of the flow distribution quality among the piled PCFCs. Increasing *a* factor will decreases the slop of the air flow distribution line. Thus, it's not like bigger *a* is better. An overlarge *a* factor will decrease the flow distributing uniformity of PCFC stack.

Table 2. Stack uniformity index for the PCFC stacks with different manifolds radii and *a* factors.

Factor *a*	Stack uniformity index	r_{in}=3 mm	r_{in}=4 mm
r_{out}/r_{in}=1	*U*	0.54	0.74
r_{out}/r_{in}=1.2	*U*	0.77	0.89
r_{out}/r_{in}=1.4	*U*	0.90	0.95
r_{out}/r_{in}=1.6	*U*	0.86	0.96

3.4 The influences of the feed/exhaust header width on PCFC stack performance
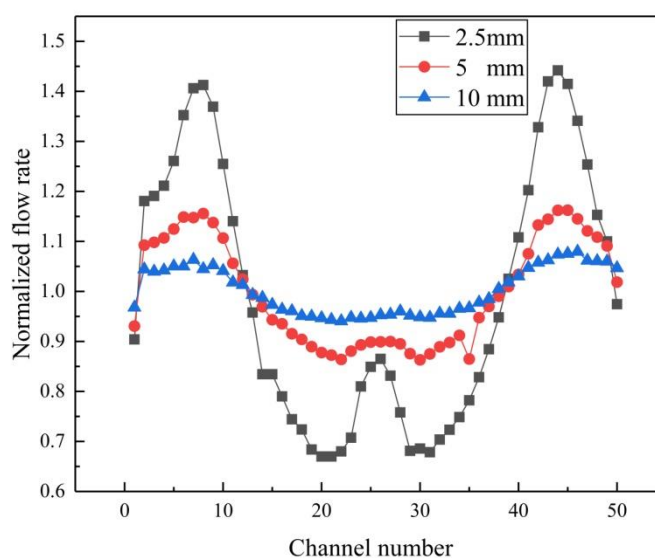
Figure 7. Normalized flow rate distributions among the rib channels over the cathode surface.

Fig. 7 further shows the normalized flow rate feeding to the rib channels over the cathode surface of 25-th PCFC unit, while different feed/exhaust header widths are adopted (i.e, 2.5, 5 and 10 mm). Obviously, the flow distribution uniformity among the rib channels will be greatly influenced by the feed/exhaust header width. The rib channels nearby the two exits of the outlet manifolds will have most of the air flow rates. Two middle rib sections (i.e. 20 and 30 channels), which far away from the exits of the outlet manifolds, will obtain fewer air flows. Increasing the width of feed/exhaust headers can greatly improve the quality of air flow distribution among rib channels over the cathode surface. This result is consistent with that obtained based on the SOFC stack [32]..

4. CONCLUSION

The 3D CFD models for the PCFC stacks are completed to study the relationship between the geometric parameters and the air flow distributing characteristics within the PCFC stacks.

i) The flow distributing uniformity will be greatly decreased with the increasing cell number of the PCFC stack. As the vapors are produced within the cathode air flow path of PCFC stack, it will also decrease the air flow distributing uniformity.

ii) Not matter the stack structures, increasing the manifold radius can relief the difference of feeding air flow rates among the piled PCFC units and decrease the total pressure drop throughout the whole stack.

iii) Increasing *a* factor of PCFC stack will decrease the slop of the air flow distribution line. Thus, it's not like bigger *a* is better. For a small manifold radius, the slops of the flow distributing line will changed greatly, while *a* factor is adjusted. For a large manifold radius, however, the slops of the flow distributing line will changed more gently, while *a* factor is adjusted.

iv) Although increasing the feed/exhaust header width will increase the flow distributing uniformity over the cathode surface of each PCFC unit, its effect on the flow distribution among the piled PCFC units is negligible.

References

1.   K. Li, T. Araki, T. Kawamura, A. Ota, Y. Okuyama. *Int. J. Hydrogen Energy*, 45 (2020) 34139.
2.   W.M. Yan, M.S. Zeng, T.F. Yang, C.Y. Chen, M. Amani, P. Amani. *Int. J. Hydrogen Energy*, 45 (2020) 22324.
3.   G. Yang, C. Su, H. Shi, Y. Zhu, Y. Song, W. Zhou, Z. Shao. *Energy & Fuels*, 34 (2020) 15169.
4.   N. Russner, S. Dierickx, A. Weber, R. Reimert, E. Ivers-Tiffée. *J. Power Sources*, 451 (2020) 227552.

5.   C. Duan, J. Huang, N. Sullivan, R. O'Hayre. *Appl. Phys. Rev.*, 7 (2020) 011314 .
6.   Q. Zhang, Y. Guo, J. Ding, G. Jiang, J. Wen. *J. Power Sources*, 472 (2020) 228232.
7.   K.J. Albrecht, A. Dubois, K. Ferguson, C. Duan, R.P. O'Hayre, R.J. Braun. *J. Electrochem. Soc.*, 166 (2019) F687.
8.   E.K. Shin, E. Anggia, A.S. Parveen, J.-S. Park. *Int. J. Hydrogen Energy*, 44 (2019) 31323.
9.   N. Wang, S. Hinokuma, T. Ina, C. Zhu, H. Habazaki, Y. Aoki. *J. Mater. Chem. A*, 8 (2020) 11043.
10. S.H. Hwang, S.K. Kim, J.T. Nam, J.S. Park. *Int. J. Hydrogen Energy*, 46 (2021) 1076.
11. Z. Zhu, S. Wang. *Ceram. Int.*, 45 (2019) 19289.
12. J. Zhao, Q. Jian, Z. Huang, L. Luo, B. Huang. *J. Power Sources*, 435 (2019) 226775.
13. C. Duan, R.J. Kee, H. Zhu, C. Karakaya, Y. Chen, S. Ricote, A. Jarry, E.J. Crumlin, D. Hook, R. Braun, N.P. Sullivan, R. O'Hayre. *Nature*, 557 (2018) 217.
14. Y. Okumura, Y. Nose, J. Katayama, T. Uda. *J. Electrochem. Soc.*, 158 (2011) B1067.
15. L.Q. Le, C.H. Hernandez, M.H. Rodriguez, L. Zhu, C. Duan, H. Ding, R.P. O'Hayre, N.P. Sullivan. *J. Power Sources*, 482 (2021) 228868.
16. S. Choi, C.J. Kucharczyk, Y. Liang, X. Zhang, I. Takeuchi, H.I. Ji, S.M. Haile. *Nat. Energy*, 3 (2018) 202.
17. Q. Shen, S. Li, G. Yang, N. Huang. *J. Electrochem. Sci.*, 14 (2019) 5344.
18. D. Chen, K. Ding, Z. Chen, T. Wei, K. Liu. *Energy Convers. Manage.*, 178 (2018) 190.
19. D. Chen, B. Hu, K. Ding, C. Yan, L. Lu. *Energies*, 11 (2018) 1875.
20. D. Chen, Y. Xu, B. Hu, C. Yan, L. Lu. *Energy Convers. Manage.*, 171 (2018) 807.
21. S. Maharudrayya, S. Jayanti, A.P. Deshpande. *J. Power Sources*, 157 (2006) 358.
22. Y. Zou, J. Li, J. Zhang, K. Ding, H. Wen. *Ionics*, 25 (2019) 4851.
23. T. Yuan, X. Wu, S.J. Bae, X. Zhu. *Reliab. Eng. Syst. Saf.*, 189 (2019) 157.
24. D. Medvedev. *Int. J. Hydrogen Energy*, 44 (2019) 26711.
25. X.V. Nguyen, G. B. Jung, S. H. Chan. *J. Electrochem. Sci.*, 14 (2019) 9132.
26. C. Duan, J. Tong, M. Shang, S. Nikodemski, M. Sanders, S. Ricote, A. Almonsoori, R. O'Hayre, *Science*, 349 (2015) 1321.
27. S. Su, H. He, D. Chen, W. Zhu, Y. Wu, W. Kong, B. Wang, L. Lu. *Int. J. Hydrogen Energy*, 40 (2015) 577.
28. D. Chen, Y. Xu, M.O. Tade, Z. Shao. *ACS Energy Lett.*, 2 (2017) 319.
29. D. Chen, H. Wang, S. Zhang, M.O. Tade, Z. Shao, H. Chen. *AlChE J.*, 61 (2015) 3786.
30. W. Bi, D. Chen, Z. Lin. *Int. J. Hydrogen Energy*, 34 (2009) 3873.
31. S. Su, S. Zhang, C. Yan, Z. Yang, F. Zheng, L. Zhang. *Int. J. Electrochem. Sci.*, 12 (2017) 230.
32. D. F. Chen, Z. Y. Chen, J. Li, J. Q. Zhang, K. Liu. *Int. J. Electrochem. Sci.*, 14 (2019) 2857